Statistical azimuthal structuring of the substorm onset arc: implications for the onset mechanism

AGU PUBLICATIONS

Geophysical Research Letters

RESEARCH LETTER
10.1002/2016GL071826

Key Points:
- The overwhelming majority of seemingly homogenous substorm onset arcs have characteristic azimuthal spatial structuring
- Characteristic spatial scales of these auroral beads are quantitatively calculated in the range 80–105 km in the ionosphere
- Consistent structuring of the onset arc is compelling statistical evidence that a plasma instability is a critical component of the substorm

Supporting Information:
- Supporting Information S1
- Figure S1

Correspondence to:
N. M. E. Kalmoni,
nadine.kalmoni.13@ucl.ac.uk

Citation:
Kalmoni, N. M. E., I. J. Rae, K. R. Murphy, C. Forsyth, C. E. J. Watt, and C. J. Owen (2017), Statistical azimuthal structuring of the substorm onset arc: Implications for the onset mechanism, *Geophys. Res. Lett.*, *44*, 2078–2087, doi:10.1002/2016GL071826.

Received 4 NOV 2016
Accepted 14 FEB 2017
Accepted article online 18 FEB 2017
Published online 4 MAR 2017

Statistical azimuthal structuring of the substorm onset arc: Implications for the onset mechanism

N. M. E. Kalmoni[1], I. J. Rae[1], K. R. Murphy[2], C. Forsyth[1], C. E. J. Watt[3], and C. J. Owen[1]

[1]Mullard Space Science Laboratory, University College London, Dorking, UK, [2]NASA Goddard Space Flight Center, Greenbelt, Maryland, USA, [3]Department of Meteorology, University of Reading, Reading, UK

Abstract The onset of an auroral substorm is generally thought to occur on a quiet, homogeneous auroral arc. We present a statistical study of independently selected substorm onset arcs and find that over 90% of the arcs studied have resolvable characteristic spatial scales in the form of auroral beads. We find that the vast majority (~88%) of auroral beads have small amplitudes relative to the background, making them invisible without quantitative analysis. This confirms that auroral beads are highly likely to be ubiquitous to all onset arcs, rather than a special case phenomena as previously thought. Moreover, as these auroral beads grow exponentially through onset, we conclude that a magnetospheric plasma instability is fundamental to substorm onset itself.

1. Introduction

The fundamental interaction between solar wind with a southward magnetic field and the oppositely orientated magnetospheric field results in magnetic reconnection on the dayside magnetopause which causes a buildup of open magnetic flux and storage of energy in the magnetotail lobes [*McPherron*, 1970]. The substorm expansion phase is the subsequent explosive release of this stored energy and is traditionally identified in the ionosphere by "a sudden brightening of the most equatorward auroral arc, or the sudden formation of a new arc which rapidly brightens and expands" [*Akasofu*, 1964, 1977]. The magnetospheric processes which drive these large-scale auroral dynamics, and the sequence in which they happen, are widely disputed. The two predominant substorm models are based on whether the substorm is initiated by processes such as instabilities at the inner edge of the plasma sheet [e.g., *Lui*, 1991; *Roux et al.*, 1991] or with tail reconnection at the near-Earth neutral line [e.g., *Hones*, 1976; *Baker et al.*, 1996].

Magnetosphere dynamics can be remotely sensed through space and ground-based auroral campaigns [*Shiokawa et al.*, 1996; *Mende et al.*, 2000, 2008; *Angelopoulos*, 2008; *Motoba et al.*, 2012]. These have enabled detailed studies of the morphology of substorm aurora and revealed the complexity of substorm dynamics initially reported by *Akasofu* [1964, 1977]. Structures known as auroral rays or beads have been observed to form azimuthally along the substorm onset arc in the minutes before auroral substorm onset [*Davis*, 1962; *Henderson*, 1994]. In recent years there have been many studies of auroral beads from data acquired by high resolution (temporal and spatial) ground-based all-sky imagers (ASIs) [e.g., *Friedrich et al.*, 2001; *Kepko et al.*, 2009; *Sakaguchi et al.*, 2009; *Rae et al.*, 2009, 2010; *Motoba et al.*, 2012; *Murphy et al.*, 2014; *Kalmoni et al.*, 2015] in which beads are reported to have spatial scales, or wavelengths, in the range 30–150 km in the ionosphere. *Sakaguchi et al.* [2009] reported two case studies of substorm onset arcs which exhibited beading with spatial scales of 30–60 km in the ionosphere. This scale closely corresponds to the ion gyro radius of 1–10 keV protons in the plasma sheet at 10 R_E, where the magnetic field strength is ~12 nT. *Motoba et al.* [2012] observed beads with wavelengths of 30–50 km at magnetically conjugate stations in the Northern and Southern hemispheres, confirming that the source of the beads is most likely in the equatorial magnetosphere. There have also been multiple substorm studies in which auroral beads were not reported [e.g., *Angelopoulos et al.*, 2008; *Nishimura et al.*, 2010] leading to a general consensus that auroral beads are only part of the auroral substorm sequence in a small subset of substorms.

Typically, the formation of auroral beads at substorm onset has been associated with the development of a plasma instability in the inner magnetosphere prior to the onset of reconnection in the tail [e.g., *Rae et al.*, 2009; *Murphy et al.*, 2014; *Kalmoni et al.*, 2015]. *Rae et al.* [2009] showed that auroral beads in the ionosphere and coincident ULF Pi1-2 wave activity preceded auroral breakup. In the absence of any observational evidence for the occurrence of reconnection, these authors concluded that a near-Earth magnetospheric

instability developed before the onset of reconnection in the tail. Using ground-based and multipoint in situ data, *Murphy et al*. [2014] presented a detailed analysis of two consecutive substorms and demonstrated that the development of auroral beads and disturbances in the inner magnetosphere preceded any evidence of tail reconnection further away from the Earth. *Kalmoni et al*. [2015] presented a statistical study of auroral substorm onset arcs with clear, visually identified, auroral beads. The authors demonstrated that, for all of these arcs, the auroral brightness grew exponentially with time for a common range of spatial scales, suggesting these are evidence of wave processes in the magnetosphere. This exponentially growing auroral beads signature is indicative of plasma instability [e.g., *Rae et al*., 2010]. The statistically dominant magnetospheric spatial scales of $k = 2.5–3.75 \times 10^{-6}\,\mathrm{m}^{-1}$ and growth rates of ~$0.05\,\mathrm{s}^{-1}$ obtained by *Kalmoni et al*. [2015] are consistent with both the shear-flow ballooning instability [*Voronkov et al*., 1997] and the cross-field current instability [*Lui*, 2004] at the inner edge of the plasma sheet, with the majority of events mapping to 9–12 R_E in the magnetotail.

In this paper we present a quantitative analysis of 195 independently identified onset arcs in order to investigate whether azimuthal structuring is a common feature of all substorm onset arcs. Although the majority of arcs may visually appear homogeneous, through detailed, quantitative analysis we demonstrate that well-defined spatial scales are detectable in at least 90% of onset arcs.

2. Methods

In this study we used data from the ASIs associated with the NASA Time History of Events and Macroscale Interactions during Substorms (THEMIS) mission [*Angelopoulos*, 2008; *Mende et al*., 2008] to quantitatively and statistically characterize the azimuthal structure of auroral onset arcs. An example of the analysis technique used to make this characterization is shown in Figure 1. Figure 1a shows an isolated auroral substorm observed at the center of the Fort Yukon ASI on 9 February 2007. The three images show the evolution from a faint auroral arc at 10:16:00 UT to a highly structured bright arc at 10:17:00 UT, resulting in auroral breakup at 10:17:30 UT. Near-midnight auroral arcs are typically aligned with constant geomagnetic latitude, whereas away-from-midnight auroral arcs become skewed, deviating from constant latitude contours by as much as 20° [*Gillies et al*., 2014]. Since substorm onset typically occurs in the premidnight sector [*Frey et al*., 2004], the onset arc will be skewed relative to constant geomagnetic latitude. Hence, we develop an arc-finding algorithm to track the onset arc as a function of longitude through the growth and early expansion phases of the substorm, during which the arc often moves latitudinally. The arcs are tracked until auroral breakup, at which point there is no longer a discrete arc as the westward traveling surge has formed and aurora has begun to fill the night sky.

To account for latitudinal skewing of the arc, we find the position of the arc in latitude as a function of geomagnetic longitude for each image by fitting a Gaussian function to each longitudinal slice to identify the latitudinal center of the arc. Examples of the arcs determined by this method are outlined in white/black in Figure 1a. The arc is most clearly visible in the earliest frame shown and does not change orientation appreciably in the subsequent frames. Figure 1b shows the logarithm of the total auroral intensity in the whole field of view of the Fort Yukon imager for the duration of the event. The total auroral intensity is used to determine auroral substorm onset, our zero epoch time, for this statistical study. We use the start time of large-scale exponential growth of the total auroral intensity in the field of view of the ASI as our definition for auroral substorm onset. Substorm onset has thus been identified as 10:16:33 UT for this event (second vertical line in Figures 1b–1e), using a linear fitting technique in log-space to determine the start time at which the data are best represented by a linear trend (see supporting information S1).

In order to investigate the azimuthal structuring of the auroral arc, the auroral intensity for the latitudinally moving arc (equatorward during the growth phase and poleward during the expansion phase) is used to create an along-arc (azimuthal) keogram as a function of geomagnetic longitude. Figure 1c shows the along-arc keogram for the moving arc identified by the arc-finding algorithm described above. On close inspection of the keogram, auroral beading, indicated by faint repeating features of higher intensity moving Westward (to lower longitudes), is visible at longitudes above −94.0° prior to 10:16:30 UT. However, the beading signature also becomes visible in the center of the keogram after 10:16:00 UT at approximately −97.0° longitude. These beads initially move both Eastward and Westward until 10:16:33 UT (auroral onset) after which they all propagate together in the Eastward direction. We use Fourier analysis of the East-West keogram to identify

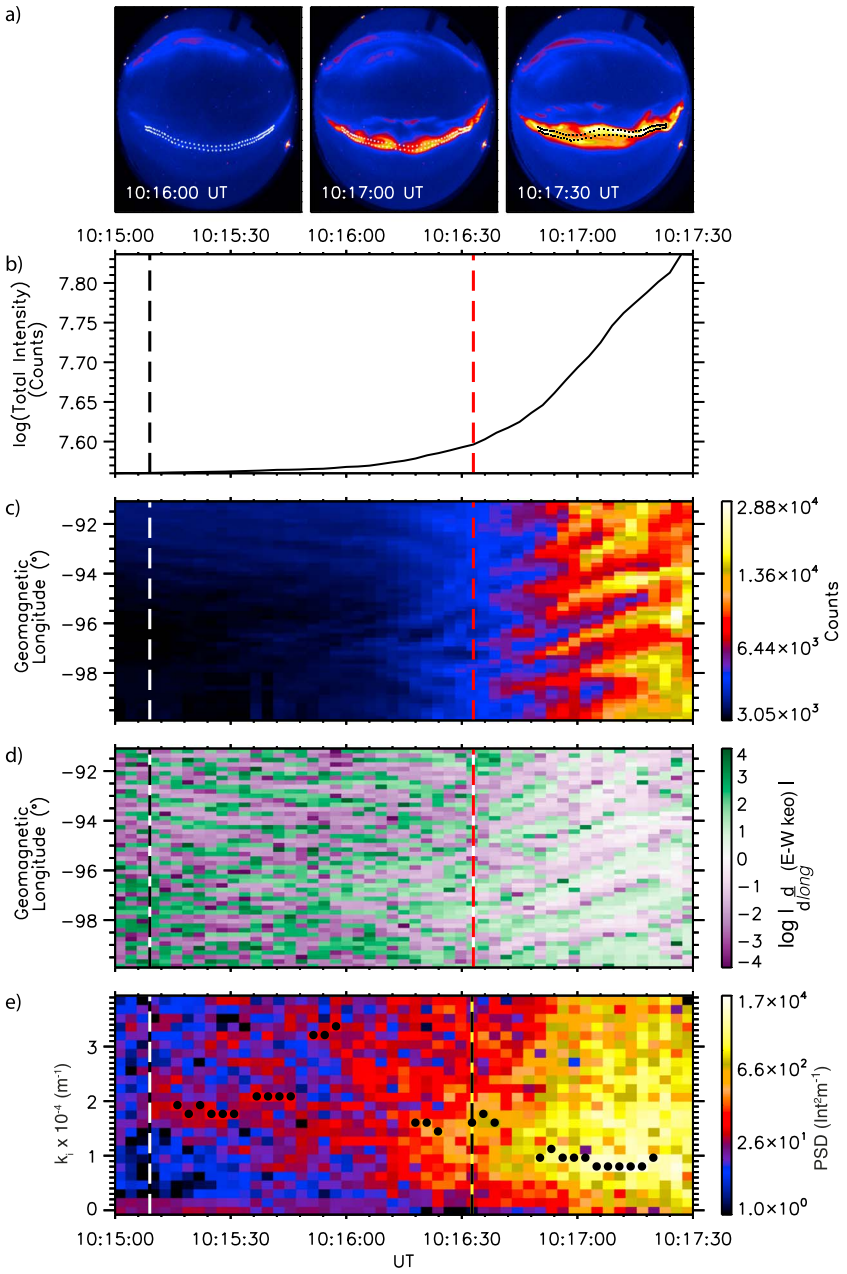

Figure 1. Auroral substorm observed from Fort Yukon all-sky imager on 9 February 2007. (a) The substorm onset arc in the minutes surrounding auroral breakup. The outline of the pixels used for analysis is shown in white/black. (b) The change in total auroral intensity from 10:15:00 to 10:17:30 UT is shown on a logarithmic scale. (c) Along-arc keogram of the auroral intensity shown in Figure 1a to show the azimuthal structure of the aurora. (d) Spatial differential of the along-arc keogram to detrend the data. (e) Dynamic PSD calculated from the differentiated keogram shown as a function of longitudinal wavenumber at 110 km altitude and time. The times and spatial scales where a clear peak in PSD is identified are indicated by the black dots.

the characteristic structuring of the onset arc. A robust characterization of the spatial scales requires the signal to be detrended without being polluted by any static background. We use along-arc numerical differentiation (with respect to longitude) to remove the background auroral arc. This allows the study of the variations in background intensity along the arc, with minimal background contributions, and hence, the resultant data set is primarily of auroral bead amplitudes only. The differentiated keogram within which the static auroral background has been removed is shown in Figure 1d. The intensity gradients

associated with the auroral beads are identified throughout the along-arc keogram by the coherent green and purple features indicating a positive and negative gradient in bead intensity, respectively. This analysis reveals the much clearer signatures of beads by the transition from green to purple in the keogram, observed at the various times and locations along the arc described above.

We apply Fourier analysis to each time point of the differentiated keogram containing signatures of the beads only (Figure 1d) using the method outlined in *Kalmoni et al*. [2015], resulting in a whitened power spectral density (PSD). We identify the temporal evolution of characteristic spatial scales from the dominant peaks of the PSD. Figure 1e shows that the PSD evolves from higher to lower wavenumbers through the late growth and early expansion phases and grows around three orders of magnitude in the process. The largest amplitude wavenumbers are marked by the black dots as a function of time. The identified dominant wavenumbers appear to be concentrated around $2\times10^{-4}\,\mathrm{m}^{-1}$ (~30 km) initially and evolve to spatial scales of ~$0.8–1.0\times10^{-4}\,\mathrm{m}^{-1}$ (~60–80 km) following substorm onset. For further details, see supporting information S1.

In this study we use the dynamic PSD to calculate to the following parameters to determine whether auroral beads are embedded within the substorm onset arc and, if so, their evolution:

1. Characteristic spatial scale: A dominant peak in PSD at a specific time indicates that there is a characteristic spatial scale embedded within the onset arc. Details on this calculation can be found in supporting information S1.
2. Time of bead onset: The time of bead onset is defined as the first time point in a 30 s sliding window where a characteristic spatial scale is identified for 80% of the time points within the window and is shown by the first vertical line in Figures 1b–1e.
3. Bead amplitude: The amplitude of each characteristic spatial scale is calculated by converting PSD to amplitude.

We note here that this quantitative analysis can also be used to determine the azimuthal motion of auroral beads which to first order would correspond to a wave phase speed. As our hypothesis is to determine whether beads are ubiquitous to all substorm arcs, we leave this to a further study.

The analysis and methodology described above is applied to 195 substorm onset arcs in order to statistically quantify the azimuthal structure of such arcs. The substorms are identified using the SOPHIE algorithm [*Forsyth et al*., 2015] from the years 2006–2014 inclusive, which identifies substorm onset from the SuperMag SML index [*Newell and Gjerloev*, 2011; *Gjerloev*, 2012] and provides an independent and unbiased substorm list from which events are selected. We also limit our study to isolated substorms that were preceded by a growth phase. For more detailed event selection criteria and additional events, see supporting information S1.

3. The Azimuthal Structuring of the Onset Arc

Figure 2 shows a superposed epoch analysis of the results for all 195 events analyzed, where auroral substorm onset is determined by the large-scale exponential brightening, as detailed in supporting information S1 and shown in Figure 1b, and corresponds to the epoch time. For the results presented in Figure 2, we use a common spatial resolution to display our statistical results, as the spatial resolution for each event is dependent upon the longitudinal extent of the auroral arc and its location in the field of view of the imager. The number of data points used to make Figures 2b and 2c are shown in Figure 2a. Note that the number of points can exceed the number of events (195) used in the study, as the individual PSDs (e.g., Figure 1e) are rebinned into a uniform common k versus time grid to create the statistical plot in Figure 2b. This means that for events with a low Nyquist frequency, multiple points from the same event can fall into the same statistical bin. In the range from -2.5 to +1 min and up to $k=3.0\times10^{-4}\,\mathrm{m}^{-1}$, there are over 100 data points per bin (shown in white in Figure 1a). This shows that the results between these values presented in Figures 2b–2d are not statistical outliers.

Figure 2b shows the median PSD, calculated from all 195 arcs as a function of wavenumber. The median PSD exhibits a peak at low wavenumbers, indicating that beads are statistically evident in the independently selected substorm onset arcs analyzed. The statistical analysis shows a tendency for PSD to peak at low characteristic wavenumbers, $k=0.4–1.2\times10^{-4}\,\mathrm{m}^{-1}$ ($\lambda=50–160$ km), with 80 km spatial scales being the most

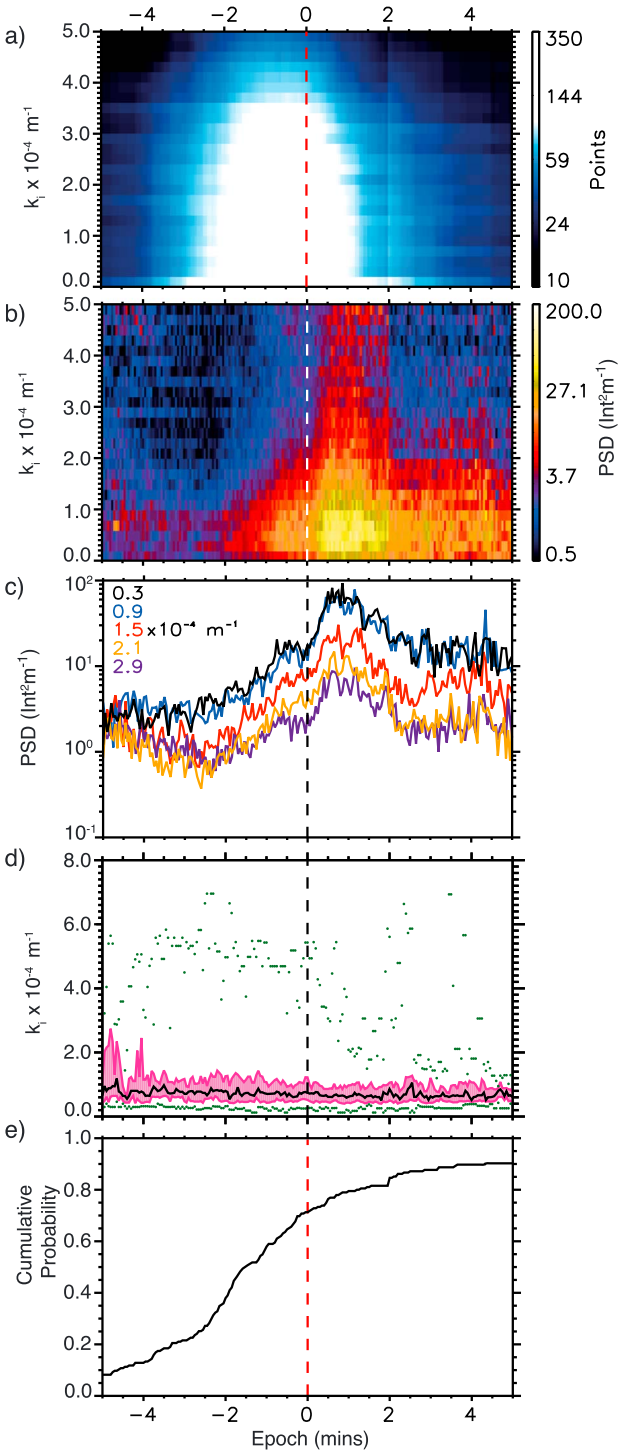

Figure 2. Statistical results from the analysis of 195 substorm onset arcs. The epoch time is auroral onset (e.g., the second vertical line in Figure 1b–1e as defined for that event). (a) Number of points in each bin. The white area indicates over 100 points/bin: this coverage is achieved from −2.5 to +1 min surrounding onset and up to $k = 3.5 \times 10^{-4}$ m^{-1}. (b) Median statistical PSD as a function of along-arc wavenumber and time. Low wavenumber are enhanced 2–3 min before auroral onset, after which all wavenumbers grow. (c) Horizontal slices of the PSD for five representative wavenumbers: $k = 0.3$ (black), 0.9 (blue), 1.5 (red), 2.1 (yellow), 2.9 (purple) $\times 10^{-4}$ m^{-1}. (d) Statistics of the peak wavenumbers identified (the black circles in Figure 1e). Median peak wavenumber as a function of time is shown by the black line, upper and lower quartiles within the pink shading. Minimum and maximum values identified for each time point are shown by the green dots. Note the extended *y* axis. (e) Cumulative probability of the bead onset time showing the proportion of events which exhibit beading relative to auroral substorm onset.

common. We note here that the broader spectral peak may be due to a combination of statistical averaging over many events and the effect of using whitened PSDs (e.g., Figure 1e) to generate this statistical plot. In general, enhancement of PSD at these wavenumbers exists 2–3 min prior to substorm onset. Around 2 min prior to substorm onset, the statistical wave power grows over a large range of spatial scales up to $k = 2.0 \times 10^{-4}\,\mathrm{m}^{-1}$.The appearance of growth at higher wavenumbers occurring later is an effect of color scale. Hence, in Figure 2c, we also show growth through specific wavenumbers to demonstrate that growth over a wide range of wavenumbers commences at approximately the same time.

The median of auroral brightness at each wavenumber shows exponential growth in the minutes before the more generally accepted definition of auroral onset, as denoted in Figure 1b. Figure 2c shows horizontal slices on a logarithmic scale through five representative wavenumbers shown in Figure 2b for $k = 0.3$, 0.9, 1.5, 2.1, $2.9 \times 10^{-4}\,\mathrm{m}^{-1}$. The overall exponential trend in PSD growth is consistent with the linear stage of plasma instability, as has been shown previously [*Rae et al*., 2010; *Kalmoni et al*., 2015]. Growth in the statistical PSD of the beads is observed prior to large-scale auroral substorm onset (Figure 1b). This is the exponential growth of the beads, which starts prior to the large-scale exponential growth of total auroral intensity (which includes both the background auroral arc intensity and the auroral beads).

We note here that Figures 2b and 2c show growth of spatial scales that are an order of magnitude smaller than the case study presented in Figure 1e. This is due to the constructing statistical averages from a highly variable physical process of substorm onset.

Figure 2d shows the statistics of the characteristic spatial scales identified using the method described in section 2 and in supporting information S1, which are denoted by the black dots in Figure 1e. The median spatial scale remains approximately constant at $k = 0.8 \times 10^{-4}\,\mathrm{m}^{-1}$ ($\lambda = 80$ km) at all epochs. There is no clear change in the median (black), upper and lower quartiles (pink), and minimum (lower dotted) values of the distributions of characteristic spatial scales before and after substorm onset. This suggests that, at least in each event, one single instability dominates for the duration of the analysis or that multiple instabilities that excite the same characteristic wavenumber must be present.

Auroral beads were detected by our automated algorithm for over 90% of events analyzed. The cumulative probability of auroral beading is shown in Figure 2e. This is calculated from the beading onsets described in section 2. Characteristic azimuthal spatial scales are detected for 70% of events prior to auroral onset. This increases to 90% at 2 min postonset, suggesting that instabilities are integral to the substorm onset process.

In order to understand why beads have previously been underreported, we examine the relative amplitude of the detected beads to the auroral arc on which they occur.

Figure 3a shows the occurrence probability of fractional bead amplitude (bead amplitude/arc intensity) as a function of arc intensity for (i) preonset and (ii) postonset times. The arc intensity is defined as the median background arc auroral intensity at that time. The increasing trend in the distribution shows that bead amplitude and arc intensity grow independently from each other.

Figure 3b shows the probability of fractional bead amplitude (bead amplitude/arc intensity) as a function of bead amplitude in the same format as Figure 3a. The distribution shows that for larger bead amplitudes, the beads constitute a larger fraction of the total arc intensity, which means that they are more easily visually identifiable. Figure 3b also demonstrates that there is a higher likelihood of high bead amplitude (ii) postonset compared to (i) preonset. This demonstrates that both absolute bead amplitudes and bead amplitude relative to the background arc intensity grow during substorm onset. Prior to substorm onset, the distribution has a tail of low bead amplitudes, which are less than 40 counts above of the background arc, and 1% of the total arc intensity (Figure 3b(i), bottom left). Very few points in the distribution have amplitudes above 2000 counts and extend above 30% of the total arc intensity (Figure 3b(i), top right). Postonset, Figure 3b(ii), it is clear from the lower left of the two-dimensional histogram that fewer events have such low bead amplitudes and that there are more events with higher bead amplitudes and fractional bead amplitudes. This shows that the bead amplitude grows through substorm onset. Clearly, the auroral arc intensity also grows. However, a change in both the absolute bead amplitude and the fractional bead amplitude between the preonset and postonset distributions demonstrates not only that there is an increase in bead amplitude during the substorm onset process but also that the bead amplitude and arc intensity grow independently from each other.

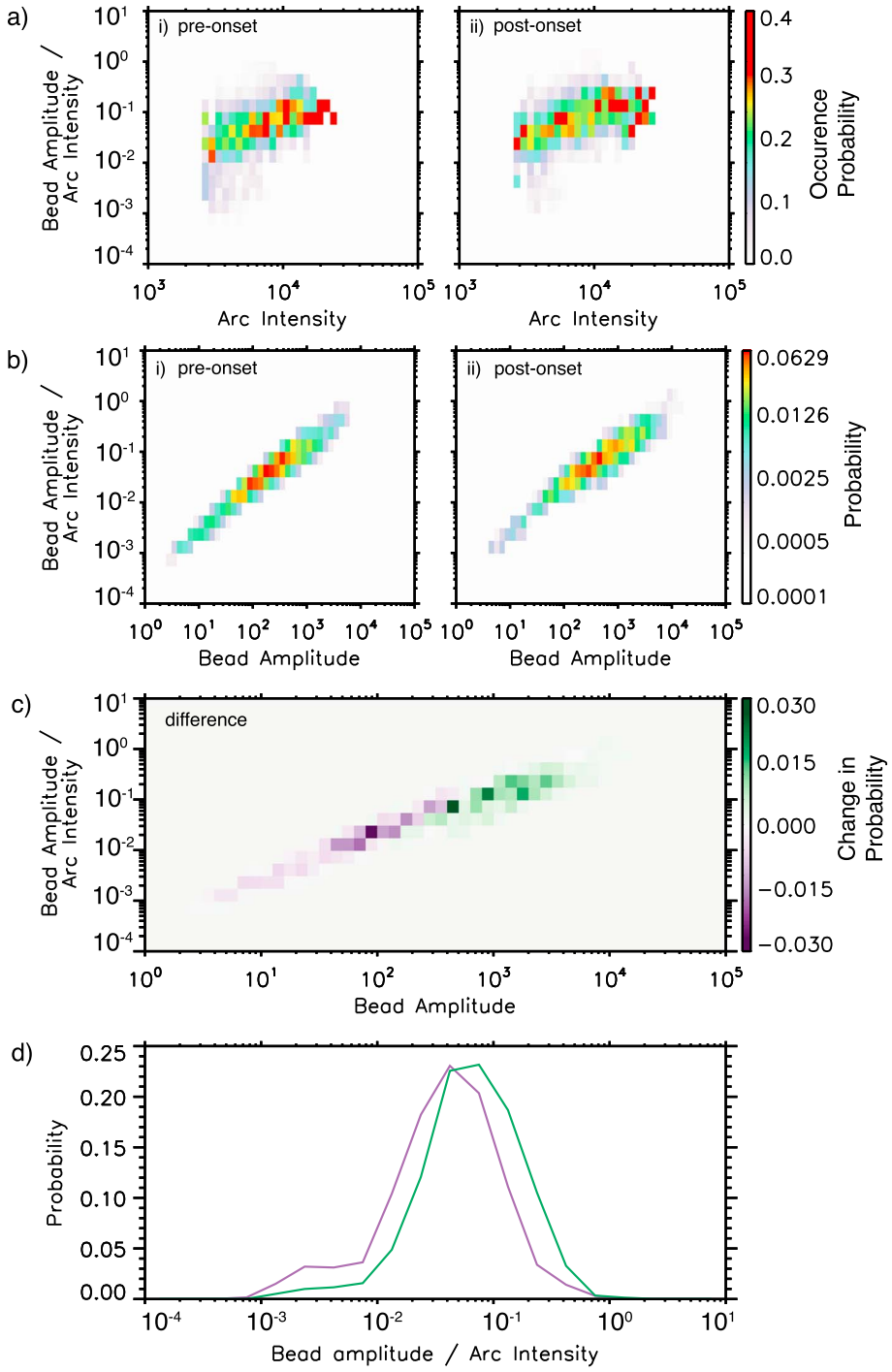

Figure 3. (a) Occurrence probability of the ratio of bead amplitude to median arc intensity as a function arc intensity for each time point where a peak wavenumber is identified (e.g., Figure 1e). Amplitude for (i) preonset and (ii) postonset times shown as a 2-D histogram. Fractional bead amplitude is lower for low arc intensity, showing bead amplitude dominates the fraction. (b) Probability of the ratio of bead amplitude to median arc intensity as a function of bead amplitude for (i) preonset and (ii) postonset times shown as a 2-D histogram. Higher counts are observed toward the lower left of the distribution prior to onset; this shifts to higher counts at higher amplitudes toward the top right of the distribution after onset. (c) Two-dimensional histogram difference between the preonset and postonset probabilities. (d) The probability distribution of the fractional bead amplitude for beads before (purple) and after onset (green).

In Figure 3c we show the difference between the preonset and postonset distributions (Figure 3b(i), (ii)). This confirms the decrease in the percentage of points in the distribution where the bead amplitude is a small fraction of the background arc intensity and an increase in the number of points where the bead amplitude is a larger fraction of the background arc intensity.

Figure 3d shows the probability distribution of the fractional bead amplitude. The fractional bead amplitude distribution prior to onset is shifted toward the higher fractional amplitudes after onset. Together with the positive gradient in Figure 3a, this change confirms that the bead amplitude and arc intensity are changing independently of each other during the onset process. Preonset, 88% of the events have beads with amplitude of less than 10% of the arc intensity; postonset, this number decreases to 76%. Despite the fact these onset arcs are *almost always* azimuthally structured, the vast majority of auroral beads have an amplitude lower than 10% of the background arc. A low fractional bead amplitude explains why beads are not frequently reported during substorms, as low amplitude beads will not be visually identified unless quantitative auroral analysis techniques, such as those described in this paper, are used.

4. Discussion

In this paper we present evidence that azimuthal structuring known as "auroral beads" is a fundamental component of the onset arc, and beads are observed in at least 90% of auroral substorms. This is the most comprehensive statistical study to date which supports theories [*Lui et al*., 1991; *Roux et al*., 1991; *Voronkov et al*., 1997; *Lui*, 2004] and previous observations [e.g., *Rae et al*., 2009; *Rae et al*., 2010; *Motoba et al*., 2012; *Kalmoni et al*., 2015] and supports that auroral beads, the ionospheric manifestation of a plasma instability, are a common and necessary process for substorm onset. However, whether the instability is initiated locally in the near-Earth tail or due to the effects of reconnection in the distant tail remains to be determined. Well-defined azimuthal structuring exists within most substorm onset arcs and grows exponentially before the large-scale classical "Akasofu" onset. This implies that a magnetospheric instability is active during the overwhelming majority of substorms in the minutes preceding global auroral brightening.

It has been shown on multiple occasions that the substorm onset arc is embedded within closed field lines in the inner magnetosphere [e.g., *Samson et al*., 1992; *Murphy et al*., 2012, 2014]. The open-closed field line boundary is defined by the poleward edge of the electron aurora [*Blanchard et al*., 1995], which is significantly poleward of the substorm onset arc and conjugate to the tail reconnection site. Auroral substorm onset occurs near the peak in the proton aurora, which is where the magnetic field topology changes from dipolar to taillike and pressure gradients develop [*Samson et al*., 1992]. Hence, this is also the region where the magnetotail is most unstable to, for example, shear-flow ballooning instability [*Voronkov et al*., 1997]. As demonstrated here, auroral beads, the ionospheric projection of the substorm onset instability, are observed prior to full auroral breakup in over 70% of substorms and during 90% of substorms within 2 min of global auroral breakup. The high prevalence of beads suggests that the instability in the inner magnetosphere develops before the classical definition of substorm onset. No other mechanisms are able to reliably describe the repeated observation of periodic auroral beads observed azimuthally along the substorm onset arc. Our results demonstrate a fundamental link between substorm onset and the development of an inner magnetospheric plasma instability.

Prior to onset, bead power is located at low wavenumbers with small amplitude fluctuations. During the end of the substorm growth phase, more magnetic flux is piled into an increasingly unstable system. Sources of free energy, e.g., large-scale pressure gradient, velocity shears, temperature anisotropies, allow quasistable waves to grow and the instability to be initiated. This can be observed in the aurora by exponential growth of auroral bead amplitudes during the linear stage of the instability [*Rae et al*., 2010; *Kalmoni et al*., 2015]. Statistically, the instability simultaneously excites exponentially growing waves over a wide range of spatial scales. *Rae et al*. [2010] and *Kalmoni et al*. [2015] demonstrate that, in individual events, specific wavenumbers grow faster than others.

Auroral beads have previously been considered to be a "special case" or statistical outlier and not a common signature of the substorm onset process. However, auroral beads are typically reported when the bead intensity is much larger than the background arc intensity, and so they are easily identifiable on visual inspection. Hence, they have been underreported prior to this study. We show that characteristic spatial scales can be identified in the vast majority of all observations with quantitative analysis; thus, auroral beads should not

be considered a special case, but rather a common feature in the auroral substorm sequence. In Figure 3 we demonstrate that, in the majority of cases studied, the bead amplitude is less than 10% of the background arc intensity. A lower ratio of bead amplitude to arc amplitude makes these characteristic spatial scales more difficult to identify without quantitative analysis, and this explains why auroral beads have not been previously reported as a regular feature of onset arcs. Bead signatures can be extremely low amplitude (Figure 3), sometimes ~40 counts or 1% of the background arc intensity. What processes result in auroral beads, and indeed what processes create the substorm onset arc, are unclear. However, we show here that bead amplitudes grow exponentially which is a classic signature of the linear stage of an instability. What process or processes drive this particular instability, how magnetosphere-ionosphere coupling operates, and how the beads relate to the substorm onset arc are all open questions that arise from our hypothesis that beads are ubiquitous to substorm onset arcs.

We note here that the spatial resolution available from the THEMIS ASIs may not always resolve the required spatial scales for beads to be resolved. Although the spatial resolution of the THEMIS ASIs corresponds to ~1 km at zenith, this resolution becomes much lower toward the horizon. At the spatial and temporal resolution of the ASIs, a beading onset time was identified for 90% of events, with 70% of events prior to auroral susbtorm onset. We propose that higher spatially resolved auroral measurements would demonstrate that beads are a universal signature along the onset arc. Hence, a plasma instability is active in the inner magnetosphere and therefore an integral component of the substorm process during the vast majority of substorms.

5. Conclusions

In this work we have presented detailed auroral analysis of the spatial structuring and dominant scales of 195 independently identified substorm onset arcs. We show that in at least 90% of events studied, auroral beads are observed along the onset arc in the minutes surrounding substorm onset. Auroral beads can statistically be observed ~2 min before auroral onset at low spatial scales and are the earliest signature of waves which exists in the near-Earth magnetosphere on closed field lines. In the minutes around auroral onset, the waves start to grow exponentially over a wide range of spatial scales; this is characteristic of the linear stage of the instability [*Rae et al*., 2010; *Motoba et al*., 2012; *Murphy et al*., 2014; *Kalmoni et al*., 2015]. During the transition from preonset to postonset times, the consistent median statistical characteristic spatial scale of the instability is indicative that a single instability is active at these times. Previously auroral beads have been underreported, because the bead amplitude is typically less than 10% of the background arc intensity, and are thus difficult to identify without quantitative analysis techniques. This is consistent with the substorm onset arc being either created, or perturbed, by an instability in the equatorial inner magnetosphere, which precedes auroral breakup by several minutes. In situ measurements are required to investigate this and determine whether the instability is initiated via external energy sources or locally at the near-Earth edge of the plasma sheet.

Acknowledgments

N.M.E.K. is supported by a Science and Technology Facilities Council (STFC) PhD studentship grant ST/K50239X/1. C. E.J.W. is supported by STFC grant ST/M000885/1. C.F. is supported by NERC IRF NE/N014480/1. K.R.M. is partially supported by an NSERC Postdoctoral Fellowship. I.J.R. and C.J.O. are supported by STFC consolidated grant to MSSL, ST/N0007722/1. I.J.R. is also supported by National Environment Research Council (NERC) NE/L007495/1. We thank Zhonghua Yao for many valuable discussions. We acknowledge NASA contract NAS5-02099 and V. Angelopoulos for use of data from the THEMIS mission. Specifically, we acknowledge S. Mende and E. Donovan for use of the ASI data, the CSA for logistical support in fielding, and data retrieval from the GBO stations and NSF for support of GIMNAST through grant AGS-1004736. The THEMIS data used in this study can be accessed at http://themis.ssl.berkeley.edu/data/themis/thg/l1/asi/. The SOPHIE substorm list is available from *Forsyth et al*. [2015] or directly from C. Forsyth upon request.

References

Akasofu, S. I. (1964), The development of the auroral substorm, *Planet. Space Sci.*, *12*(4), 273–282, doi:10.1016/0032-0633(64)90151-5.

Akasofu, S. I. (1977), Physics of magnetospheric substorms, *Astrophys. Space Sci. Lib.*, *47*.

Angelopoulos, V. (2008), The THEMIS mission, *Space Sci. Rev.*, *141*(1–4), 5–34, doi:10.1007/s11214-008-9336-1.

Angelopoulos, V., et al. (2008), Tail reconnection triggering substorm onset, *Science*, *321*(5891), 931–935, doi:10.1126/science.1160495.

Baker, D. N., T. I. Pulkkinen, V. Angelopoulos, W. Baumjohann, and R. L. McPherron (1996), Neutral line model of substorms: Past results and present view, *J. Geophys. Res.*, *101*, 12,975–13,010, doi:10.1029/95JA03753.

Blanchard, G. T., L. R. Lyons, J. C. Samson, and F. J. Rich (1995), Locating the polar cap boundary from observations of 6300 Å auroral emission, *J. Geophys. Res.*, *100*(A5), 7855, doi:10.1029/94JA02631.

Davis, T. N. (1962), The morphology of the auroral displays of 1957–1958: Detail analyses of Alaska data and analyses of high-latitude data, *J. Geophys. Res.*, *67*(1), 75–110, doi:10.1029/JZ067i001p00075.

Donovan, E., et al. (2006), The THEMIS all-sky imaging array—system design and initial results from the prototype imager, *J. Atmos. Sol. Terr. Phys.*, *68*(13), 1472–1487, doi:10.1016/j.jastp.2005.03.027.

Forsyth, C., I. J. Rae, J. C. Coxon, M. P. Freeman, C. M. Jackman, J. Gjerloev, and A. N. Fazakerley (2015), A new technique for determining Substorm Onsets and Phases from Indices of the Electrojet (SOPHIE), *J. Geophys. Res. Space Physics*, *120*, 10,592–10,606, doi:10.1002/2015JA021343.

Frey, H. U., S. B. Mende, V. Angelopoulos, and E. F. Donovan (2004), Substorm onset observations by IMAGE-FUV, *J. Geophys. Res.*, *109*, A10304, doi:10.1029/2004JA010607.

Friedrich, E., J. C. Samson, and I. Voronkov (2001), Ground-based observations and plasma instabilities in auroral substorms, *Phys. Plasmas*, *8*(4), 1104–1110, doi:10.1063/1.1355678.
Gillies, D. M., D. J. Knudsen, E. F. Donovan, E. L. Spanswick, C. Hansen, D. Keating, and S. Erion (2014), A survey of quiet auroral arc orientation and the effects of the interplanetary magnetic field, *J. Geophys. Res. Space Physics*, *119*, 2550–2562, doi:10.1002/2013JA019469.
Gjerloev, J. W. (2012), The SuperMAG data processing technique, *J. Geophys. Res.*, *117*, A09213, doi:10.1029/2012JA017683.
Henderson, M. G. (1994), Implications of Viking imager results for substorm models PhD thesis, Univ. of Calgary, Calgary, Alberta, Canada.
Hones, E. W., Jr. (1976), Observations in the earth's magnetotail relating to magnetic merging, *Sol. Phys.*, *47*(1), 101–113, doi:10.1007/BF00152248.
Kalmoni, N. M. E., I. J. Rae, C. E. J. Watt, K. R. Murphy, C. Forsyth, and C. J. Owen (2015), Statistical characterization of the growth and spatial scales of the substorm onset arc, *J. Geophys. Res. Space Physics*, *120*, 8503–8516, doi:10.1002/2015JA021470.
Kepko, L., E. Spanswick, V. Angelopoulos, E. Donovan, J. McFadden, K. H. Glassmeier, J. Raeder, and H. J. Singer (2009), Equatorward moving auroral signatures of a flow burst observed prior to auroral onset, *Geophys. Res. Lett.*, *36*, L24104, doi:10.1029/2009GL041476.
Lui, A. T. Y. (1991), A synthesis of magnetospheric substorm models, *J. Geophys. Res.*, *96*, 1849–1856, doi:10.1029/90JA02430.
Lui, A. T. Y. (2004), Potential plasma instabilities for substorm expansion onsets, *Space Sci. Rev.*, *113*(1–2), 127–206, doi:10.1023/B:SPAC.0000042942.00362.4e.
Lui, A. T. Y., C. L. Chang, A. Mankofsky, H. K. Wong, and D. Winske (1991), A cross-field current instability for substorm expansions, *J. Geophys. Res.*, *96*, 11,389–11,401, doi:10.1029/91JA00892.
McPherron, R. L. (1970), Growth phase of magnetospheric substorms, *J. Geophys. Res.*, *75*, 5592–5599, doi:10.1029/JA075i028p05592.
Mende, S. B., et al. (2000), Far ultraviolet imaging from the IMAGE spacecraft. 2. Wideband FUV imaging, *Space Sci. Rev.*, *91*(1), 271–285, doi:10.1023/A:1005227915363.
Mende, S., S. Harris, H. Frey, V. Angelopoulos, C. Russell, E. Donovan, B. Jackel, M. Greffen, and L. Peticolas (2008), The THEMIS array of ground-based observatories for the study of auroral substorms, *Space Sci. Rev.*, *141*(1–4), 357–387, doi:10.1007/s11214-008-9380.
Motoba, T., K. Hosokawa, A. Kadokura, and N. Sato (2012), Magnetic conjugacy of northern and southern auroral beads, *Geophys. Res. Lett.*, *39*, L08108, doi:10.1029/2012GL051599.
Murphy, K. R., I. R. Mann, I. J. Rae, C. L. Waters, B. J. Anderson, D. K. Milling, H. J. Singer, and H. Korth (2012), Reduction in field-aligned currents preceding and local to auroral substorm onset, *Geophys. Res. Lett.*, *39*, L15106, doi:10.1029/2012GL052798.
Murphy, K. R., I. R. Mann, I. J. Rae, A. P. Walsh, and H. U. Frey (2014), Inner magnetospheric onset preceding reconnection and tail dynamics during substorms: Can substorms initiate in two different regions?, *J. Geophys. Res. Space Physics*, *119*, 9684–9701, doi:10.1002/2014JA019795.
Newell, P. T., and J. W. Gjerloev (2011), Evaluation of SuperMAG auroral electrojet indices as indicators of substorms and auroral power, *J. Geophys. Res.*, *116*, A12211, doi:10.1029/2011JA016779.
Nishimura, Y., L. Lyons, S. Zou, V. Angelopoulos, and S. Mende (2010), Substorm triggering by new plasma intrusion: THEMIS all-sky imager observations, *J. Geophys. Res.*, *115*, A07222, doi:10.1029/2009JA015166.
Rae, I. J., et al. (2009), Near-Earth initiation of a terrestrial substorm, *J. Geophys. Res.*, *114*, A07220, doi:10.1029/2008JA013771.
Rae, I. J., C. E. J. Watt, I. R. Mann, K. R. Murphy, J. C. Samson, K. Kabin, and V. Angelopoulos (2010), Optical characterization of the growth and spatial structure of a substorm onset arc, *J. Geophys. Res.*, *115*, A10222, doi:10.1029/2010JA015376.
Rees, M. H. (1963), Auroral ionization and excitation by incident energetic electrons, *Planet. Space Sci.*, *11*(10), 1209–1218, doi:10.1016/0032-0633(63)90252-6.
Roux, A., S. Perraut, P. Robert, A. Morane, A. Pedersen, A. Korth, G. Kremser, B. Aparicio, D. Rodgers, and R. Pellinen (1991), Plasma sheet instability related to the westward traveling surge, *J. Geophys. Res.*, *96*, 17,697–17,714, doi:10.1029/91JA01106.
Sakaguchi, K., K. Shiokawa, A. Ieda, R. Nomura, A. Nakajima, M. Greffen, E. Donovan, I. R. Mann, H. Kim, and M. Lessard (2009), Fine structures and dynamics in auroral initial brightening at substorm onsets, *Ann. Geophys.*, *27*(2), 623–630, doi:10.5194/angeo-27-623-2009.
Samson, J. C., L. R. Lyons, P. T. Newell, F. Creutzberg, and B. Xu (1992), Proton aurora and substorm intensifications, *Geophys. Res. Lett.*, *19*(21), 2167–2170, doi:10.1029/92GL02184.
Shiokawa, K., et al. (1996), Auroral observations using automatic optical instruments: Relations with multiple Pi2 magnetic pulsations, *J. Geomagn. Geoelectr.*, *48*(11), 1407–1419, doi:10.5636/jgg.48.1407.
Voronkov, I. O., E. F. Donovan, and J. C. Samson (2003), Observations of the phases of the substorm, *J. Geophys. Res.*, *108*(A2), 1073, doi:10.1029/2002JA009314.
Voronkov, I., R. Rankin, P. Frycz, V. T. Tikhonchuk, and J. C. Samson (1997), Coupling of shear flow and pressure gradient instabilities, *J. Geophys. Res.*, *102*(A5), 9639–9650, doi:10.1029/97JA00386.